A Marie-Curie-ITN
within H2020

*Proceedings of the International Symposium on
Thermal Effects in Gas flows In Microscale
October 24-25, 2019 – Ettlingen, Germany*

ISTEGIM 2019 - 282727

NUMERICAL AND EXPERIMENTAL INVESTIGATION OF HEAT EXCHANGER PERFORMANCE FOR A MICRO-CHP APPLICATION

Jojomon Joseph*[1,2], Michel Delanaye[1], Danish Rehman[3], Rabia Nacereddine[1], Jan G. Korvink[2], Juergen J. Brandner[2].

[1]Mitis, Rue Bois Saint-Jean, 3, B-4102 Seraing, Belgium
[2]Karlsruhe Institute for Technology, Institute of Microstructure Technology, Karlsruhe, Germany
[3]Microfluidics Laboratory, Department of Industrial Engineering (DIN), University of Bologna, Via del Lazzaretto 15/5, 40131 Bologna BO, Italy

KEY WORDS

Micro channel, CFD methodology, Reduced model, Wire-net perturbators, S-shaped perturbators, High-temperature heat exchangers.

ABSTRACT

The objective of this paper is to investigate in detail the complex micro channel (with wire-net and S-shaped perturbators) performance and using a new CFD methodology to assess the entire heat exchanger characteristics based on reduced order modelling. Localized turbulence enhances the heat exchanger performance along with an increased pressure loss. Shifting the critical Reynolds to lower Reynolds number by using perturbators will control the pressure losses and enhance the thermal efficiency to a considerable extent. Here we consider the microchannel performance (based on thermal efficiency and pressure losses) for two different types of perturbators, Wire-net [1, 2, 3] and the S-shape [4]. The wire-net heat exchanger (Fig.1a, 1b and 1c)) is assembled as a stack of counter-flow passages with optimized thickness separated by thin foils. A metallic wire mesh is inserted in the flow passages (Fig.1c) to provide the required stiffness and enhance the microchannel efficiency (localized turbulence). The S-shaped heat exchanger model consists of S-shaped protrusions (Fig.1d and 1e) along the counter-flow passages with an integrated collector.

Microchannel performance

Three-dimensional, ideal gas, steady CHT simulations were carried out to investigate the effect of thermal efficiency and pressure losses for various inlet mass flow rates in ANSYS Fluent. Turbulent K-ω shear stress transport turbulent model was utilized for all the CHT models and collectors simulations. The free microchannel simulations were conducted using laminar models. The K -epsilon model is not accurate in the near-wall region. On the contrary, the K-ω model is appropriate for the

* joseph.jojomon@mitis.be , jojomon.joseph@partner.kit.edu

near-wall turbulent flows. Both conventional models are mixed to take advantage of both models [5]. The microchannel thermal efficiency, ε, % is calculated using the relation,

$$\varepsilon, \% \ = \frac{C_h(T_{in}^h - T_{out}^h)}{\min(C_c, C_h)\,(T_{in}^h - T_{in}^c)} \times 100 \qquad (1)$$

$$C_c = m_{\mu c} Cp_c \,;\, C_h = m_{\mu h} Cp_h \qquad (2)$$

where $Cp_{c/h}$ being the hot and cold fluid capacity rates, $T_{in/out}^h$ and $T_{in/out}^c$ are the inlet and outlet temperatures of the counter-flow channels. $m_{\mu c/\mu h}$ is the microchannel mass flow rate at hot and cold inlet. The microchannel pressure losses, ΔP, % were calculated using the relation,

$$\Delta P, \% \ = \frac{P_{in} - P_{out}}{P_{ab}} \times 100 \qquad (3)$$

Where, $P_{in/out}$is the inlet and outlet total pressure drop and P_{ab} is the absolute pressure at the inlet.

Two types of geometrical symmetry exist in a plane that is parallel to the inlet flow direction (see Fig.1a). cylindrical collectors with wire-net microchannel is shown in Fig.1a. The primary symmetrical domain (see Fig.1b) is along half of the secondary collector diameter. Besides, the secondary symmetrical domain is at the centre of the wire-net compact heat exchanger (see Fig.1c). It is computationally expensive to carry out a Conjugate Heat Transfer (CHT) analysis by holding the primary symmetry (see Fig.1b). Similarly, periodic boundary conditions were implemented in the plane that is perpendicular to the inlet flow direction. A periodicity exists in half of the microchannel foil thickness on every hot and cold side alternatively. Thus, the counter-flow arrangement is simplified into a single hot and cold microchannel with partition foil above it, as shown in Fig.1c.

Fig.2a depicts the non-dimensional velocity contours for microchannels with and without wire-net. The non-uniform velocity distribution in the microchannels (without wire-net) adversely affects the compact heat exchanger performance as mentioned by Yang et al.[6] due to the least resistance from the inlet to the outlet. This reduces the benefits of counter-flow passages since the maximum velocity gradients lie at two extreme inlets (see Fig.2a). However, the microchannels with wire-net have more homogeneous velocity distribution that retains the counter-flow effects (see Fig.2a). These effects are similar to the conventional grid turbulence theory [7] where a grid generates turbulence that is nearly homogeneous and isotropic. This is the idealized model assumed in most of the turbulence theory and most of the turbulence models [8]. Thus the numerical model was further simplified (see Fig.1c and 1e) for detailed CHT analysis.

There is an optimum mass flow rate where the thermal efficiency reaches a maximum [1, 2]. However, a substantial decrease in efficiency at higher mass flow rates has been encountered. The steepness of this efficiency curve pattern is stronger for the S-shape perturbator compared to the wire-net protrusions (see Fig. 2b). This steepness increases the working range and thereby reduces the size and cost of the compact heat exchanger. As the steepness decreases, the microchannels can work at high mass flow rates with higher efficiency and thereby the number of microchannels required will decrease. As the result, heat exchanger becomes more compact and cost-effective. However, for the wire- net (at higher Reynolds numbers) the pressure loss is relatively high. The pressure loss varying pattern (along with an increasing mass flow rate) is quadratic, which is similar to the conventional

Darcy Forschmiers Law, where the inertial and viscous term are well-balanced. The free microchannels have the least pressure losses as expected. The wire-net introduces higher pressure losses compared to S-shaped fins (see Fig.2b).

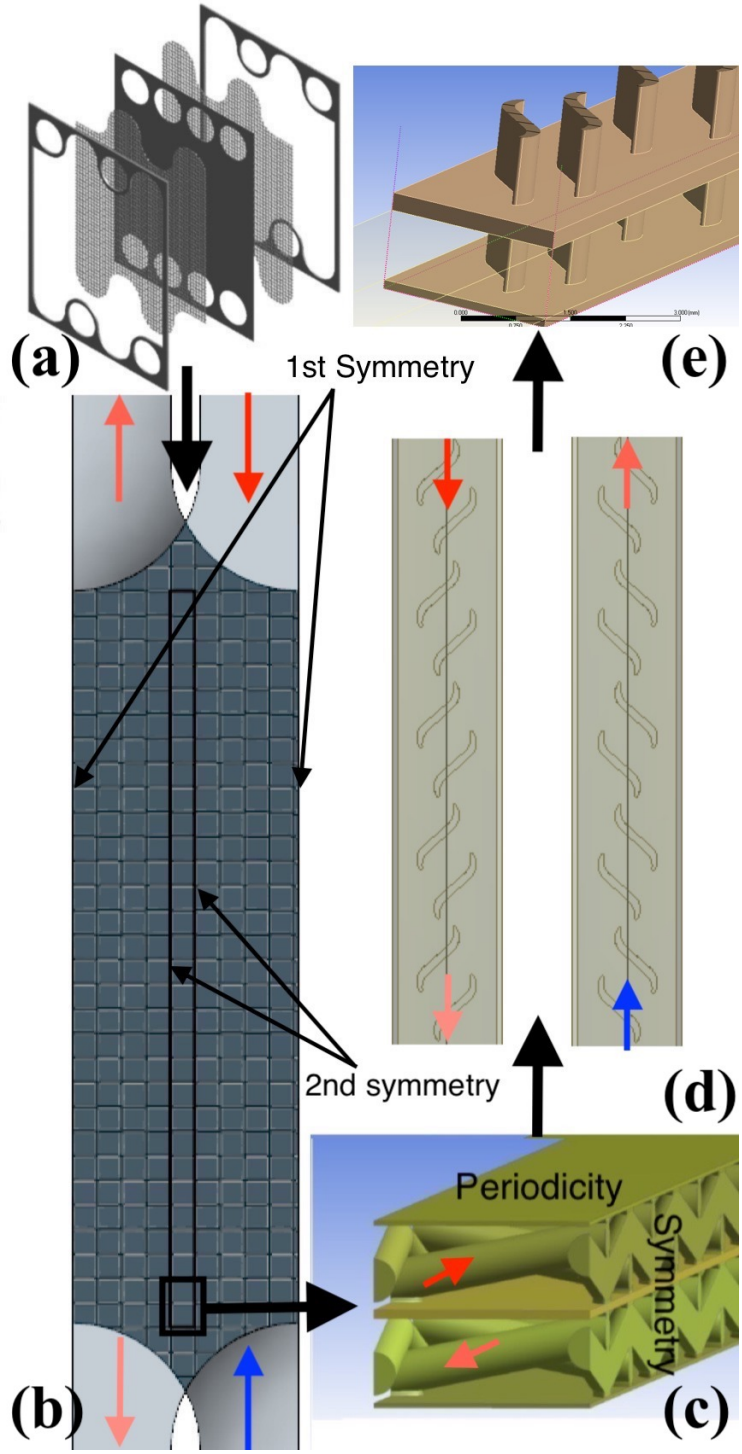

Figure 1. *(a) Wire net brazed heat exchanger Arrangement, (b) Microchannels with wire-net perturbators, (c) Conjugate Heat Transfer domain, (d) Microchannels with S-shaped perturbators,(e) Conjugate Heat Transfer domain.*

CHT analysis was conducted on microchannels with different arrangement of S-shape perturbators. The number for S-shaped fins of normal, inverted and aligned arrangements were 22, 26 and 26

respectively. Fig.3 shows the pressure loss and thermal efficiency of the microchannels with different S-shaped fin arrangement. The quadratic pressure loss curve is plotted along the secondary y-axis, and the thermal efficiency is plotted along the primary y-axis. The microchannel performance is not directly proportional to the number of fins. However, the performance is directly proportional to the flow physics. In general, the pressure losses were lowest for the case in which the S-shaped fins were inverted, which results in lower thermal efficiency as well.

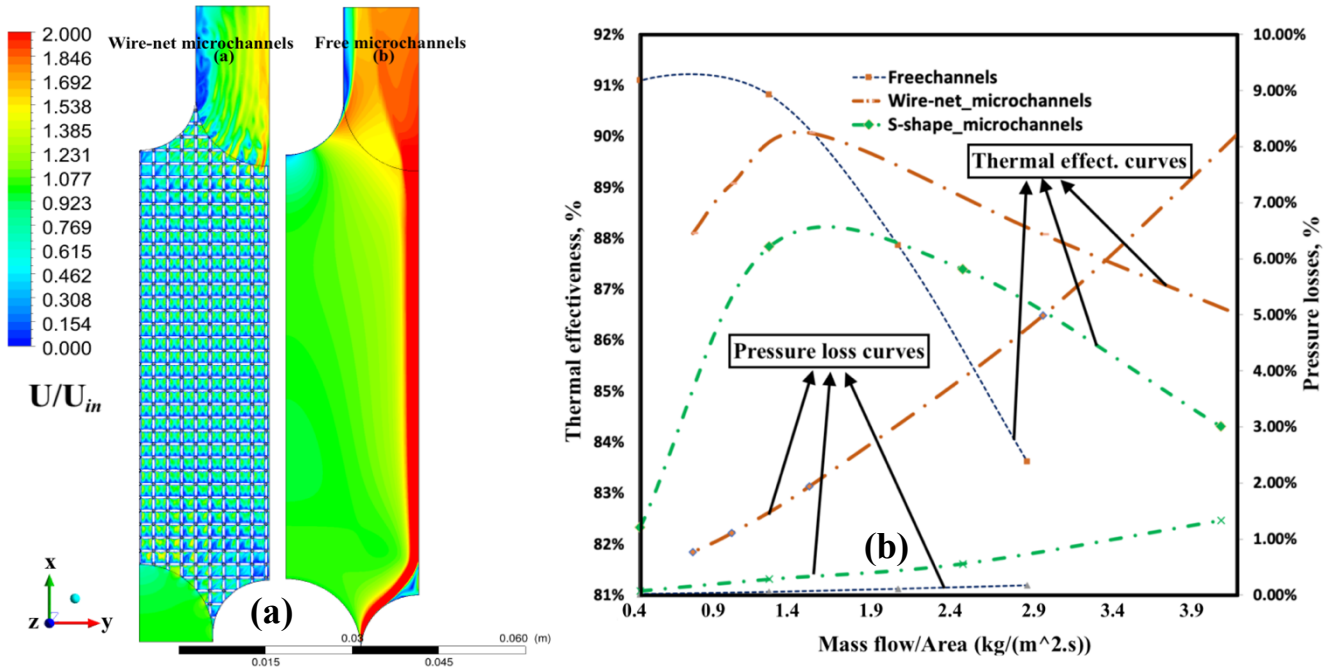

Figure 2. *(a) Non-dimensional velocity contour of microchannels with and without wire-net, (b) Thermal efficiency and pressure drop of free channels, with wire-net and S-shape microchannels for various mass flow rates.*

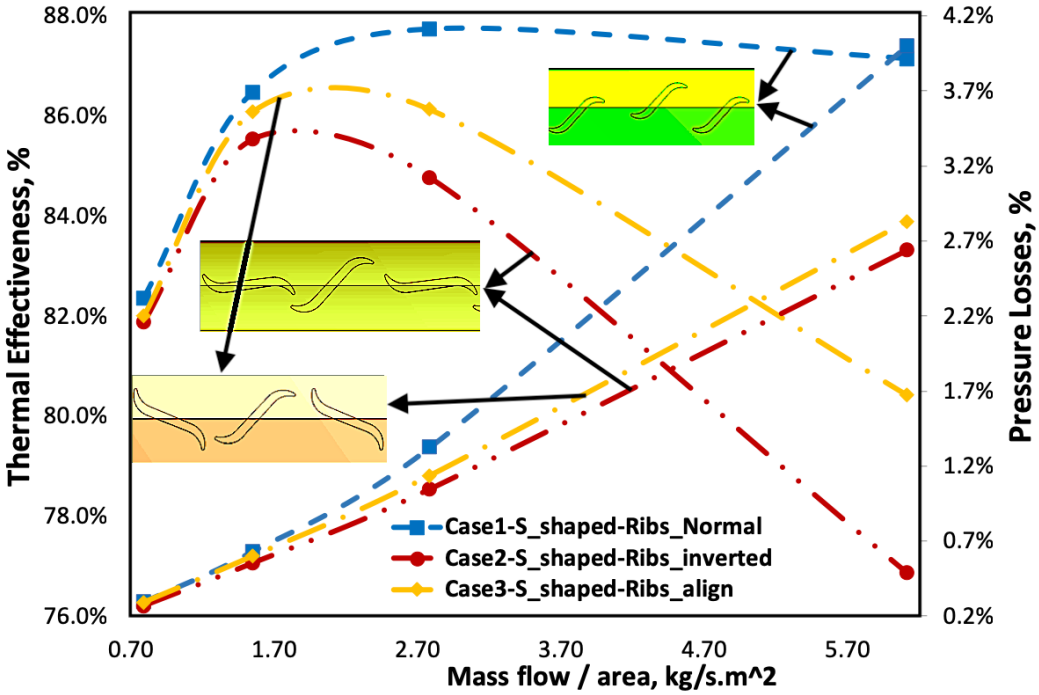

Figure 3. *Thermal efficiency and pressure losses for three different types of S-shape fin arrangements.*

Collector analysis

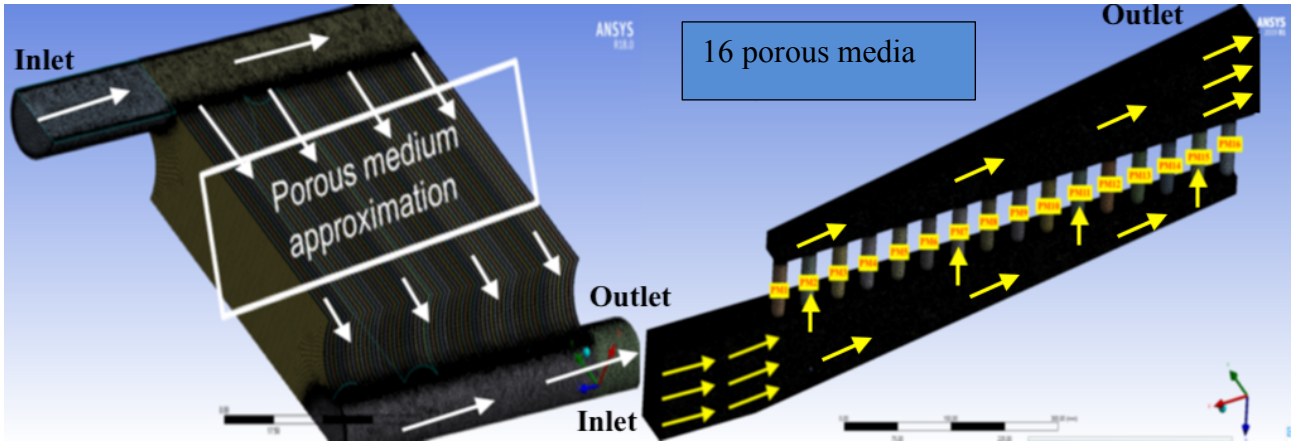

Figure 4. *(a) Secondary collector model, (b) Primary collector mesh model with 16 porous media which replicates 16 collectors.*

A CFD methodology was utilised (presented in paper Joseph et al. [1, 2] for the collector analysis. The primary and secondary collector mesh model is depicted in Fig.4a and 4b, respectively. Half section of the cylindrical collectors that feed 60 microchannels is depicted in Fig.4a. Trapezoidal primary collectors distributed the flow to 16 secondary collector inlets and illustrated in Fig.4b. Apparently, a cylindrical channel with porous medium approximation replaces the effects of secondary collector and microchannels. The microchannels of the wire-net/S-shape fins have a complicated structure, which makes the numerically expensive to simulate. The best method is to split the heat exchanger configuration part by part and analyze the performance using Reduced Order Modelling (ROM). An outline of the CFD methodology is shown in Fig.5a. Secondary collectors mass flow rate is defined as the deviation from the ideal CHT inlet mass calculated using the relation,

$$m_{\mu CHT} = \frac{m_{co}}{\gamma\, n_{pl}} \tag{4}$$

$m_{\mu CHT}$ is the microchannel mass flow rate, m_{co} is the collector mass flow rate,
n_{pl} is the number of plates/channels and γ is the microchannel size reduction coefficient,
calculated because of simplification of computational domain (symmetric and periodic BCs). For primary collectors, its defined as the ideal secondary collector mass flow rate calculated using,

$$m_{co} = \frac{m_{to}}{2n_{bl}} \tag{5}$$

m_{co} is the secondary collector mass flow rate, m_{to} is the total mass flow rate and
n_{bl} is the number of blocks/exchangers

The modelling is performed in three different stages:

1. Microchannel Conjugate Heat Transfer model – Estimating the microchannel performance using detailed three-dimensional CHT analysis.
2. Reduced model for secondary collectors– Microchannels are replaced by porous medium models to evaluate the flow maldistribution and thereby the secondary collector performance. Therefore, the microchannels are having a very coarse mesh (10 000 cells per channels), and the secondary collector has a highly refined mesh to capture the secondary effects.
3. Reduced model for primary collectors– Scalability of the ROM is utilized to model both microchannel along with the secondary collectors as a single porous medium. Therefore, the effects of both microchannels and secondary collectors were introduced into a cylindrical duct. The cylindrical duct has a very coarse mesh, and the primary collector has a highly

refined mesh. An overall heat exchanger performance is estimated based on the flow maldistribution and overall pressure losses.

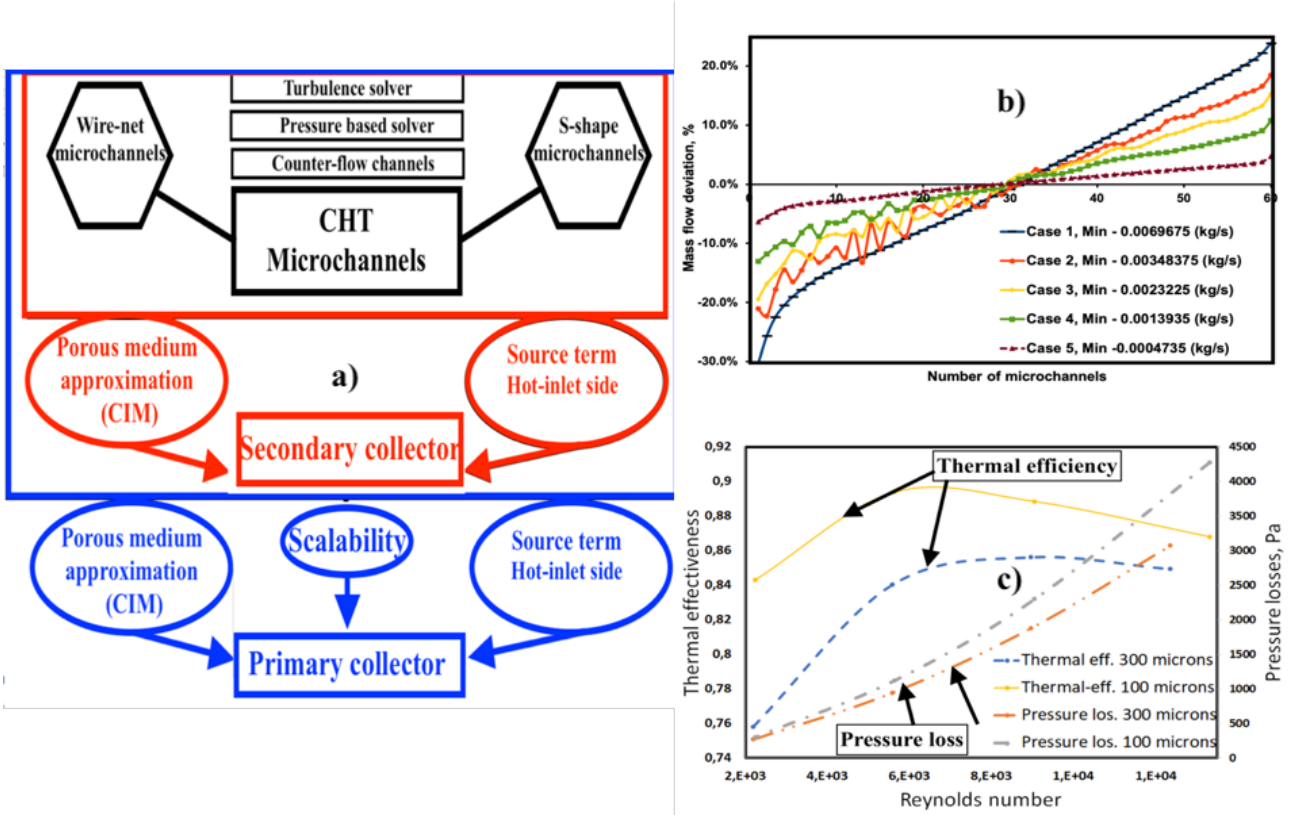

Figure 5. *(a) Scheme for CFD methodology, (b) Mass flow rate distribution, (c) Secondary collector performance with different microchannel foil thickness*

In the first stage of the CFD modelling, a detailed CHT analysis is carried out for a microchannel section with specific boundary conditions. Microchannel performance characteristics are utilized to model the microchannels as porous media with inertial and viscous coefficients as the main parameters. In the second stage of modelling, the microchannels are considered as porous media, and the secondary collector performance is evaluated. Constant Integration Method (CIM) based on Darcy-Forchheimer law was utilized to calculate the porous medium characteristics which replicated the conjugate heat transfer model. The computational domain is sharply reduced since the microchannels are examined as porous media with free-slip boundary condition.

In the third stage of modelling, the microchannels with collectors are considered as porous media, and the scalability of the ROM provides the easiness to create the temperature and pressure jump across different type of cross-sections. Scalability of the ROM is developed to characterize the primary collector performance and thereby the overall heat exchanger performance for the micro CHP system.

Porous medium

The global parameters such as pressure drop, thermal efficiency, and turbulent viscosity are determined from three-dimensional CHT analysis of microchannels. This is utilized to calculate the inertial and viscous coefficients (porous medium model) of the reduced model using CIM. The Darcy-

Forchheimer law was modified and implemented to account for the large temperature variation ($\Delta T = 600\ K$) and localized turbulence effect in the microchannels [1],

$$\frac{(P_{in} - P_{out})}{L} = \frac{1}{\alpha}\frac{L}{\Delta T}\frac{m}{A}\frac{R}{P}\left\{\left[T^{\frac{1}{2}}(3T^2 - 5S_1T + 15S_1^2) - 15S_1^{\frac{5}{2}}\arctan\left(\frac{T}{S_1}\right)^{\frac{1}{2}}\right) + \epsilon_m\frac{PT}{R}\right]_{T_0}^{T_1} + \frac{1}{2}C_2\frac{m}{A}\left[\frac{T^2}{2}\right]_{T_0}^{T_1}\right\} \quad (6)$$

Power per unit volume was implemented as a source term along the microchannels (see Eq.(6)). Joseph et al. [1] implemented the new approach and validated the porous media model (with modified inertial and viscous coefficients) for secondary collectors.

$$Q = m_{\mu CHT}(T_{in}^{h/c} - T_{out}^{h/c})Cp_{h/c} \quad (7)$$

The model is validated numerically and experimentally [1, 2, 3]. Rehman et al. [9] used similar approach for microchannels with large density variations (compressible flows). The collector's flow maldistribution influences the mass flow rate and thereby the heat transfer prediction is biased along with total pressure losses.

Collector performance

Secondary collector

The secondary collectors distribute the flow to 60 microchannels and the flow maldistribution is depicted in Fig.5b. The collectors with a higher mass flow rate have a maximum deviation from the ideal CHT mass flow rate. Studies made by Thansekhar et al. [10] and Teng et al.[11] showed that, higher the flow resistance through the channels better is the flow distribution among the channels. From there studies, at higher flow rates, the flow distribution becomes more uniform and also the flow resistance increases with the increased mass flow. As the mass flow rate increases, the microchannel pressure loss also increases. Apparently, the static pressure rise in the secondary collector is not relatively high at higher microchannel mass flow rates. Thus the collectors maintain uniform pressure in the collectors, resulting in a low maldistribution.

Partition foil thickness with 100 and 300 microns was selected for secondary collector performance analysis. An overall thermal efficiency for each collector inlet mass flow rate is calculated as the mass flow rate-weighted average thermal efficiency of all microchannels and plotted in Fig.5c. The overall pressure losses is extracted directly from the ROM model for specific operating condition and depicted in Fig.5c. The quadratic increase in pressure loss is evident from the microchannel analysis. The thermal efficiency is higher for the 100 microns configuration. As the partition foil thickness decreases, the thermal efficiency is enhanced for a counter-flow arrangement [6].

Fig.6a shows the Lambda 2.velocity, vorticity strength of the recirculation zone for three different mass flow rates. The vortices originate at the beginning of the recirculation zone and remain steady enough to dissipate the integral vortex near the collector beds. Due to the intense mixing of the recirculating fluid with the entraining fluid, strong vortices originate along the recirculation zone. The intensity of the recirculation zones of the cylindrical collector is evident from the vorticity contour (see Fig.6a). Thus the mass flow rate has a strong effect on flow maldistribution. As the resistance inside the microchannel increases, the vorticity strength increases. The mass flow rate distribution

near the collector beds become irregular, and deviation from the CHT mass flow rate increases with an increase in collector inlet mass flow rate (see Fig.5b).

Primary collector

The primary trapezoidal collector inlet distributes the flow to 16 secondary collectors and then to 60 microchannels. Collector flow maldistribution strongly depends on the secondary flows in the primary collectors. Parametric study on different primary collector heights were conducted and the flow maldistribution is depicted in Fig.6b. As the collector height increases, the maldistribution decreases and the optimum collector height is found to be at 100 mm. The velocity contour of minimum and maximum collector heights is represented in Fig.6c and 6d) respectively. As the height increases, the velocity near the secondary collector inlets decreases, and the recirculation strength also decreases. The highest turbulence production for the maximum height configuration is near the primary collector outlet. The small collector height primary collector configuration has profoundly influenced the flow distribution as well as the turbulence characteristics.

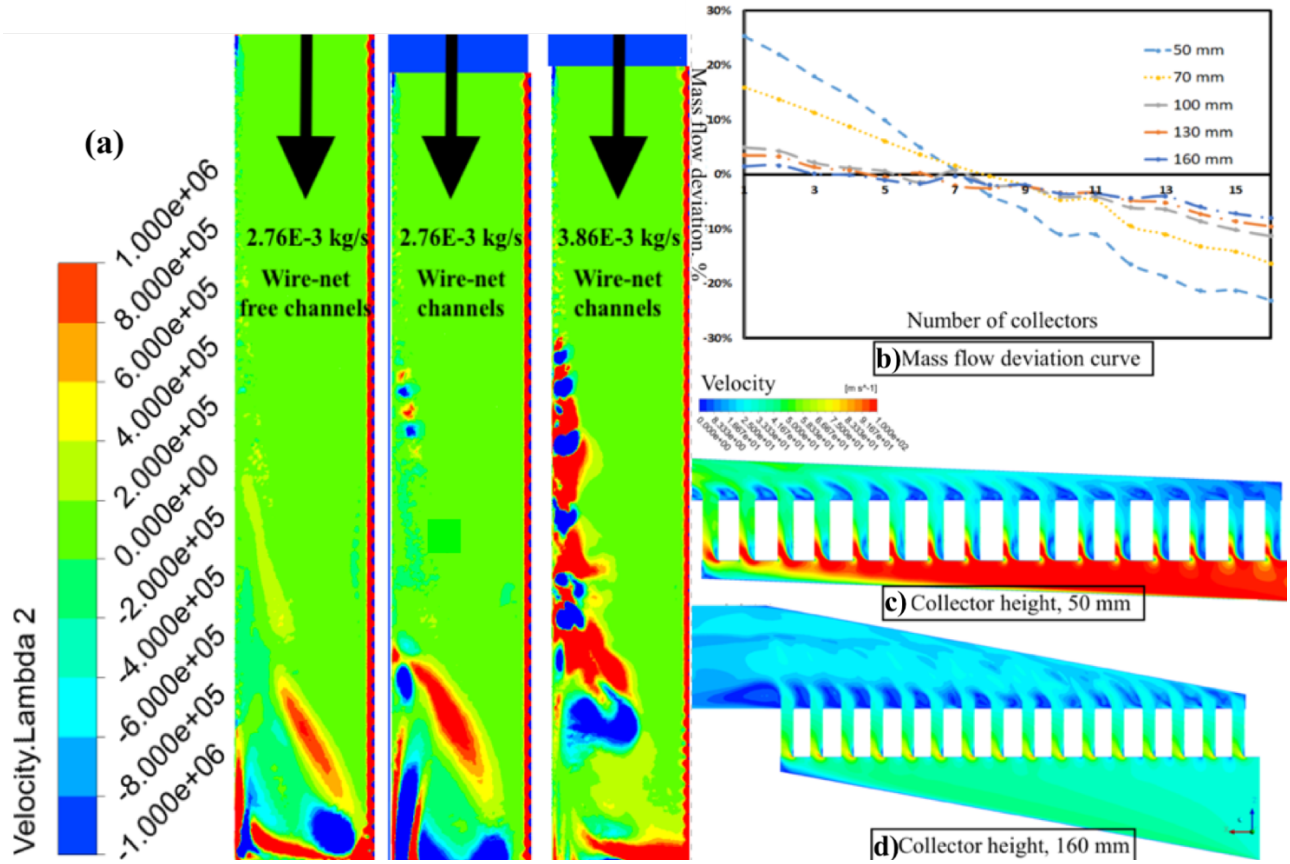

Figure 6. *(a) Secondary collector performance for different heights, (b) velocity contour height= 50 mm, (c) velocity contour height= 160 mm,*

Experimental testing

A mass flow rate controller with an operating range of 0-5000 NmL/min controlled the mass flow rate inlet. The facility is equipped with three flow meters having a different operative range. We switch from one controller to another tank to a three-way valve in order to obtain the desired Reynolds number inside the channel with the best precision. The total pressure drop between the inlet and the

outlet of the microchannel assembly is measured utilizing a differential pressure transducer (Validyne DP15) with an interchangeable sensing element that allows accurate measurements over the whole range of encountered pressures. Atmospheric pressure is measured using an absolute pressure sensor (Validyne AP42). The pressure sensor calibration is performed using a comparison test pump (Giussani BT 400), which is capable of imposing the desired pressure difference relative to the atmosphere. The analog voltage signal from DP sensors is amplified and is fed to an internal multiplexer board of Agilent 49470A and then read employing the Labview program. To measure the temperature at the entrance of the microchannel a K-type, the calibrated thermocouple is used. Thermocouple voltage and an amplified voltage of pressure sensors are fed to the internal multiplexer board of Agilent 39470A and are read through a PC using a Labview program.

Test bench for microchannels with S-shaped perturbators are depicted in Fig.7a. The microchannels were tested for a regime of mass flow rates. It was found that the critical Reynolds number has shifted to lower Reynolds number. Deviation of laminar friction factor to turbulent friction factor (from Blasius profile) occurred at Re=180, see Fig.7b. This is in good agreement with several studies conducted by Shah and Wanniarachchi [12], Heggs et al. [13], Focke et al. [14] and Liu and Tsai [15] on corrugated plate heat exchanger microchannel geometries. For Shah, the Reynolds critical was less than 200, while Heggs suggested that the flow is never laminar after Re= 150. The rest authors suggested the Reynolds critical is in between Reynolds number 300 and 400. The length scale (roughness, perturbators size) of the microchannels disturbances determines the turbulent transition. If the length scale is too small, the turbulent transition occurs at the conventional Reynolds number. When length scale increases, the critical Reynolds number reduces to smaller Reynolds number.

Apart from that, secondary collector together with the microchannel configuration was tested. It was fabricated using 3D printing (plastic). Six pressure taps which were installed for pressure readings (see Fig.8a). Five pressure taps were installed near the microchannel inlets, and the remaining one was placed at the collector inlet. The size of the pressure tap hole was 60 microns, and it was ensured that the pressure taps were placed precisely at the center of the duct, see Fig.8a. The test was carried out to investigate the collector pressure losses and compare it with CFD. The results between CFD and microchannel is depicted in Fig.8b. There is a good agreement between CFD and experiments and the relative error is less than 4 %.

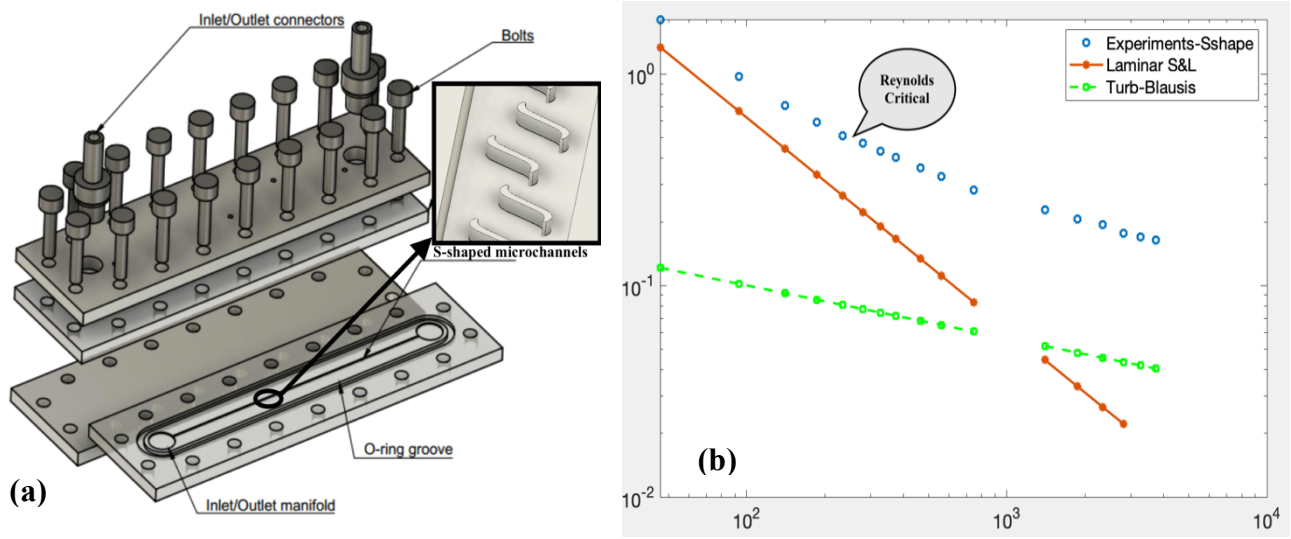

Figure 7. *(a) Experimental test bench for S-shaped microchannels, (b) Friction factor for various Reynolds number*

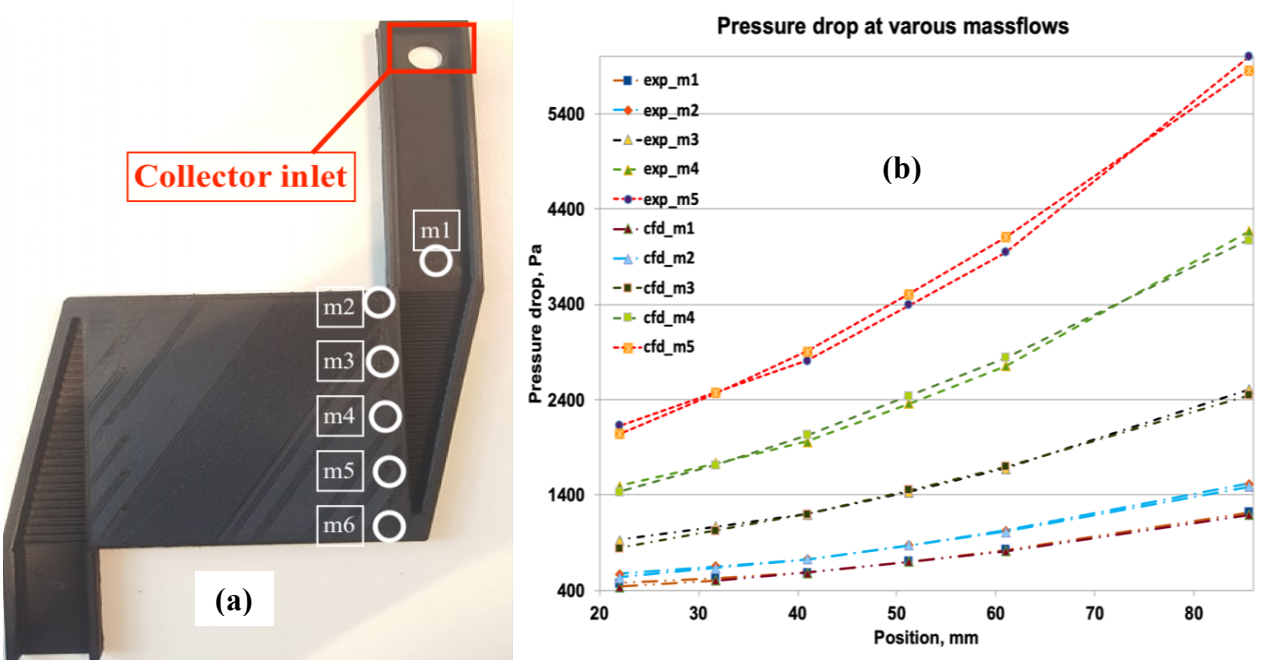

Figure 8. *(a) Experimental test design for collector flow maldistribution (b) Comparison plot between experimental and CFD pressure losses.*

Conclusion

The wire-net microchannels have a better performance in terms of thermal efficiency. On the contrary, S-shape fins have a better performance in terms of pressure losses. The wire-net produced more pressure losses relative to S-shape and plane channels. The wire-net geometry suppresses the separation and reduces the size of flow detachment zones lowering the pressure losses with an enhanced heat transfer.
Collector performance assessed using the ROM showed that the flow maldistribution increases as the microchannel pressure drop decreases. The strength of the recirculation zone near the collector beds was suppressed at higher mass flow rates. Higher the primary collector height, lower the maldistribution, and thereby, thermal efficiency and pressure drop is enhanced. There is an optimum height where the pressure loss is saturated, and the non-uniformity in maldistribution is relatively less (for different primary collector heights). Experimental testing showed that the turbulent transition occurred at very low Reynolds number due to the effect of perturbators. Apart from that, the collector simulation results coincided with the experimental results with good accuracy (< 4%.).

Nomenclature

A – cross-sectional area, m^2
BCs - Boundary conditions
CFD - computational fluid dynamics
CHP - combined heat and power
CHT - conjugate heat transfer
CHE - compact heat exchanger
$Cp_{c/h}$ - heat capacity at constant pressure for cold/hot inlet microchannels, $\frac{J}{K}$
C_c - cold fluid capacity rate, $\frac{W}{K}$

C_h - hot fluid capacity rate, $\frac{W}{K}$
L - microchannel length, mm
$m_\mu, m_{\mu c}, m_{\mu h}$- microchannel mass flow for cold/ hot inlet channels, $\frac{kg}{s}$
m_{co} - collector inlet mass flow for cold/hot inlet side, $\frac{kg}{s}$
$m_{\mu CHT}$ - microchannel mass flow calculated from CHT model inlet, $\frac{kg}{s}$
n_{pl} - number of plates
PM – porous medium
P, P_{in}, P_{out}, P_{ab} – inlet/ outlet total pressure and absolute pressure, Pa
ROM - reduced order model
R - universal gas constant, $\frac{J}{mol\ k}$
S_l - Sutherland constant
T – temperature, K
$T_{in,out}^{h,c}$ - inlet and outlet total temperatures for hot \- cold microchannel inlets and outlets, K
ΔT - temperature drop across the microchannel length, K
ΔP - pressure drop across the length, Pa
Q – thermal source term, $\frac{W}{m^3}$
U, U_{in}- stream wise mean velocity, inlet velocity, $\frac{m}{s}$

Greek Symbols

$1/\alpha$ - viscous coefficient, m^{-2}
β - inertial coefficients, m^{-1}
γ - microchannel size reduction coefficient
ρ - density, kg/m^3
ε - thermal efficiency, %
ϵ_m- turbulent viscosity, $m^2.s^{-1}$

Acknowledgements

This ITN Research Project MIGRATE (www.migrate2015.eu) is supported by European Community H2020 Framework under the Grant Agreement No. 643095. The research of MITIS has been funded by grants Nanocogen+ and Nanocogen+2 from DGO4 and DGO6 directorates of Wallonia.

References and Citations

[1] J. Joseph, M. Delanaye, R. Nacereddine, J.J. Brandner and J. G. Korvink, "Advanced numerical methodology to analyze high-temperature wire-net compact heat exchangers for a micro-combined heat and power system application", *Heat Transfer Engineering* pp. 1-13, July, 2019. DOI:10.1080/01457632.2019.1589984

[2] J. Joseph, M. Delanaye, R. Nacereddine, A. Giraldo, M. Rouabah, Jan G. Korvink and J. J. Brandner. Numerical and experimental investigation of a wire-net compact heat exchanger performance for high-temperature applications. Applied Thermal Engineering, 154:208– 216, 2019.

[3] M. Delanaye, A. Giraldo, R. Nacereddine M. Rouabah V. Fortunato and A. Parente. Development of a recuperated flameless combustor for an inverted bryton cycle microturbine used in residential micro-chp. ASME. Turbo Expo: Power for Land, Sea, and Air, 4B:Charlotte, North Carolina, USA,, June 26–30.

[4] N. Tsuzuki, M. Utamura, T. LamNgo, Nusselt number correlations for a microchannel heat exchanger hot water supplier with S-shaped fins. appl. Therm. Eng., 29:3299–3308, 2009.

[5] R. Manceau, Industrial codes for CFD, International masters in turbulence, Applied Mathematics Departement, Inria-Cagire group, CNRS–University of Pau, Pau, France, 1 edition, 2017, [Online]. Available:http://remimanceau.gforge.inria.fr/Publis/PDF/IndustrialCodesForCFD.pdf. Accessed: May. 23, 2019.

[6] Y. Yang. Experimental and Numerical Analysis of Gas Forced Convection through Microtubes and Micro Heat Exchangers. PhD thesis, Ingegneria Energetica, Nucleare e del Controllo Ambientale, UNIBO, Italy, 2013.

[7] Gersten Klaus Schlichting, Hermann. Boundary-Layer Theory. Springer-Verlag Berlin Heidelberg, Germany, 9 edition, 2017.

[8] Grid turbulence. http://www.lfpn.ds.mpg.de/turbulence/generation.html.

[9] D. Rehman, G. L. Morini, J. Joseph, M. Delanaye, J. Brandner. A porous media model for a double-layered gas-to-gas micro heat exchanger operating in laminar flow regime. UIT Heat Transfer Conference 2019, 2019.

[10] M.R. Thansekhar C. Anbumeenakshi. Experimental investigation of header shape and inlet configuration on flow maldistribution in microchannel. Experimental Thermal and Fluid Science, 75:156–161, 2016.

[11] M.S. Liu C.C. Wang R. Greif J.T. Teng, J.C. Chu. Investigation of the flow mald- istribution in microchannels, in: Proceeding of the asme congress. IMECE41323, 2:465–469, 2003.

[12] B. Thonon P. Tochon R. Shah, M. Heikal. Progress in the numerical analysis of compact heat exchanger surfaces. Adv. Heat Transf., 42:363–443, 2001.

[13] R. Hallam C. Walton P. Heggs, P. Sandham. Local transfer coefficients in corru- gated plate heat exchanger channels. Chem. Eng. Res. Des., 75:641–645, 1997.

[14] I. Olivier W. Focke, J. Zachariades. The effect of the corrugation inclination angle on the thermohydraulic performance of plate heat exchangers. Int. J. Heat Mass Transf., 28:1469–1479, 1985.

[15] Y.C. Tsai F.B. Liu. An experimental and numerical investigation of fluid flow in a cross-corrugated channel. Heat Mass Transf., 46:585–593, 2010.